



TRACE-Python: Tracer-based Rapid Anthropogenic Carbon Estimation Implemented in Python (version 1.0)

Daniel E. Sandborn¹, Brendan R. Carter², Mark J. Warner¹, and Larissa M. Dias^{2,3}

¹School of Oceanography, University of Washington, Seattle, WA, USA

²Cooperative Institute for Climate, Ocean, and Ecosystem Studies, University of Washington, Seattle, WA, USA

³NOAA Pacific Marine Environmental Laboratory, Seattle, WA, USA

Correspondence: Daniel E. Sandborn (sandborn@uw.edu)

Abstract. An implementation of Tracer-based Rapid Anthropogenic Carbon Estimation (TRACE), an algorithm for estimating anthropogenic carbon in the ocean, was produced using the Python coding language. TRACE is a transit time distribution approach intended to increase the accessibility of reliable and accurate anthropogenic carbon estimates. This algorithm produces estimates of ocean anthropogenic carbon as a function of user-supplied coordinates, year, depth, seawater salinity, atmospheric carbon dioxide pathway, and optionally seawater temperature. We demonstrate the identical results of this implementation relative to its MATLAB predecessor, explore the sensitivity of anthropogenic carbon estimates to a newly-expanded range of available user input parameters, and suggest further lines of development for this software product as well as transient tracer-based ocean state estimation in general. Additionally, a new column integration routine was developed and deployed on anthropogenic carbon estimates generated from TRACE-Python when applied to the GLODAPv2.2016b gridded product 10 temperature and salinity, yielding updated global and regional anthropogenic carbon inventories for the industrial era through the year 2500 along a range of atmospheric carbon dioxide trajectories. These inventories demonstrate satisfactory agreement with previous observation-based anthropogenic carbon inventories within the uncertainty of the estimate, demonstrating the skill of the TRACE method at the global level. This implementation of TRACE represents a step forward in accessibility to a wider user base, flexibility in user-specification of a greater number of estimation parameters, and skill as measured against 15 other anthropogenic carbon estimates.

1 Introduction

Anthropogenic carbon in the ocean (C_{anth}) is defined as the increase in dissolved inorganic carbon (DIC) in seawater attributable to anthropogenic carbon dioxide (CO_2) emissions to the atmosphere over the industrial era. As the ocean is the largest single historical sink of CO_2 (Friedlingstein et al., 2023) and is expected to absorb most of the anthropogenic CO_2 transient on 20 millennial scales (Archer et al., 1998), understanding the distribution and rates of change of C_{anth} in the global ocean is central to informing climate change (DeVries et al., 2023). On local scales, accumulation of C_{anth} gains further relevance as a driver of ocean acidification and other ecosystem disruptions that affect important natural resources (Doney et al., 2020). These disruptions underlie the need for accurate and accessible methods for estimating C_{anth} in the ocean.



Several methods for inferring C_{anth} from observational data have been devised. These may be separated into two classes:
25 back-calculation and inversion. Back-calculation methods such as the ΔC^* (Gruber et al., 1996) and eMLR(C^*) (Clement and Gruber, 2018) techniques seek to estimate C_{anth} accumulation as a function of various measurable chemical parameters by removing changes in inorganic carbon system observations since water mass formation or an earlier set of measurements. These techniques have informed an improved understanding of the ocean carbon sink based on repeat hydrographic observations, but suffer from the inability to extrapolate to unobserved periods, and the reliance on assumptions that complicate their
30 interpretation including transient steady state invasion of anthropogenic signals, fixed nutrient and carbon stoichiometries, and simplified mixing models (Khatiwala et al., 2013; Müller et al., 2023).

In contrast, inversion-based methods infer the propagation of a surface response to anthropogenic atmospheric CO_2 throughout the ocean by means of circulation constrained by measurements of chlorofluorocarbons (CFCs), sulfur hexafluoride (SF_6), and other transient tracers of ocean circulation (Hall et al., 2002; Haine et al., 2025), taking advantage of similarities between
35 the atmospheric histories of these anthropogenic gases (Figure 1). Inverted ocean tracer transport may be projected backwards and forwards in time (if one assumes steady state circulation and knowledge of atmospheric inventories), providing opportunities to explore changes in the ocean carbon sink (Khatiwala et al., 2009) and oxygen utilization (Sonnerup et al., 2015). Additionally, some inventory estimates have combined elements of both back-calculation and inversion methods (Sabine et al., 2004).

40 One subclass of the inversion-based methods, the Transit Time Distribution (TTD), relies on a Green's function solution of the linear advection-diffusion transport equations to provide an age distribution representing water mass ages (Hall et al., 2002). The functional form of a TTD age distribution may vary, but an inverse-gaussian (IG) function specified using its first and second moments (Γ and Δ ; Equation 1) has been shown to describe the tracer transport regimes of many ocean regions well in comparison with ocean general circulation models when provided with optimal parameters (He et al., 2018).

$$45 \quad \mathcal{G}(t) = \sqrt{\frac{\Gamma^3}{4\pi\Delta^2 t^3}} e^{-\frac{\Gamma(t-\Gamma)^2}{2t\Delta^2}} \quad (1)$$

This function describes one-dimensional pipe flow along isopycnal surfaces from a single source region. Other formulations of the age distribution may represent more complex mixing regimes (Holzer and Primeau, 2010). Despite the demonstrated utility of TTD methods for unraveling ocean tracer transport as well as recent calls for development of C_{anth} estimations based on transient tracers (Müller et al., 2023), their complex formulation and implementation has historically restricted their use.
50 To overcome this barrier to more accessible science, an implementation of a TTD method was given by Carter et al. (2025) as “Tracer-based Rapid Anthropogenic Carbon Estimation version 1” (hereafter TRACEv1). Among the limitations of that implementation was its formulation using MATLAB (which while open-source is not freely available), and its dependence upon predetermined surface boundary conditions and TTD shape.

To address these limitations, this work describes an update of the Tracer-based Rapid Anthropogenic Carbon Estimation
55 routine and its implementation in the Python coding language. A brief overview of inherited methods is given followed by a description of new aspects of this implementation of TRACE, which encompass both practical improvements and fundamental

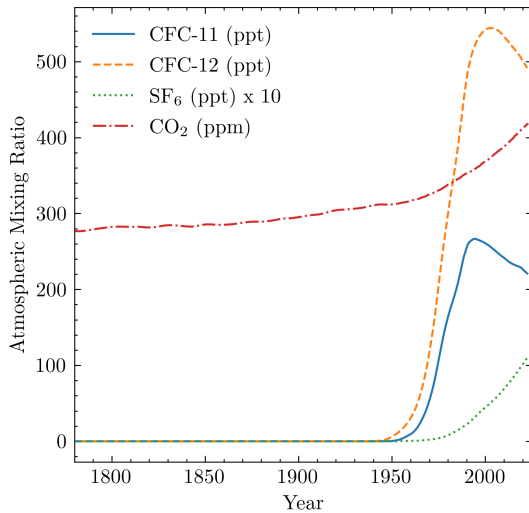


Figure 1. Atmospheric history of CO₂ and transient tracers CFC-11, CFC-12, SF₆ given as mixing ratios over 1780 to present. Transient tracers are given as global means of northern and southern hemisphere annual mean values from Bullister and Warner (2017). CO₂ is from the Mauna Loa time series (Keeling and Keeling, 2017) since 1958 and from the Law Dome reconstruction (Rubino et al., 2019) for earlier dates. Units are indicated in the legend as parts per million (ppm) or parts per trillion (ppt); note scaling of SF₆ by 10x to render it visible.

changes to the method. This routine is validated against TRACEv1 to establish exact comparability, then used to produce an updated global gridded C_{anth} data product using an updated integration routine. A sensitivity analysis is then carried out to explore the effect of practical improvements to the TRACE method. Finally, we consider this method's strengths, limitations, 60 and future development.

2 Summary of Inherited Methods

This implementation of TRACE in Python is both an exact replication of its TRACEv1 predecessor's results as well as an improvement in function. Equivalent results of this work and the original TRACEv1 and the effect of improvements are described in Section 4. It inherits the IG-TTD method implemented by its MATLAB-based predecessor in form and function, 65 which is briefly described here, along with the convolution of the resulting water mass ages with an atmospheric boundary condition and calculation of inferred C_{anth}. Hereafter, we use "TRACE" to refer to the algorithm, "TRACEv1" to refer to its implementation in MATLAB, and "TRACE-Python" to refer to its implementation in Python, for which this study used version 1.0.0. More detailed information about the TRACE method and its oceanographic context can be found in our previous work (Carter et al., 2025).

70 TRACE first estimates an age distribution for seawater from user-provided geographic coordinates, depth, salinity, and (optionally) temperature using a neural network trained on ages inferred by IG-TTD from paired CFC-11, CFC-12 and SF₆ observations as well as the mean water mass age estimates from the Ocean Circulation Inverse Model (DeVries, 2014). The



shape of the IG-TTD (as specified by its first moment Γ and second moment Δ) was not allowed to vary from $\Delta/\Gamma = 1.3$; however, TRACE-Python makes this available as a user parameter, as described in Section 3.1.

75 User specification of an atmospheric CO₂ pathway allows convolution of the age distribution with a surface boundary condition to yield $p\text{CO}_2$. This is converted to DIC via inorganic carbon equilibrium calculation with preformed total alkalinity, preformed phosphate ion, and preformed silicate ion estimated by separate neural networks (Carter et al., 2021b). Subtracting preindustrial DIC (calculated assuming a preindustrial atmospheric mixing ratio of 280 ppm and the same preformed properties) leaves C_{anth}. Built-in atmospheric CO₂ pathways include eight shared socioeconomic pathways (SSPs): 1-1.9, 1-2.6, 80 2-4.5, 3-7.0, 3-7.0-lowNTCF, 4-3.4, 4-6.0, and 5-3.4 (Meinshausen et al., 2020) and historical data with a linear extrapolation of the present increase (denoted Historical/Linear), all spanning the years 1-2500 c.e. TRACEv1 estimated the C_{anth} surface boundary condition partial pressure of carbon dioxide ($p\text{CO}_2^{\text{oce}}$) at a time t (in years) as a recursive function of the time-varying atmospheric CO₂ mixing fraction $x\text{CO}_2^{\text{atm}}(t)$:

$$p\text{CO}_2^{\text{oce}}(t) = x\text{CO}_2^{\text{atm}}(t) - 0.144 \times (x\text{CO}_2^{\text{atm}}(t) - x\text{CO}_2^{\text{atm}}(t - 65)) \quad (2)$$

55 This was derived as an empirical relationship between atmospheric and surface ocean trends in a model-observation hybrid product (Jiang et al., 2023), and it defines a surface boundary responsive to both the atmospheric value and the rate of atmospheric increase or decrease. This ad-hoc boundary condition formulation is retained by TRACE-Python, and its contribution to TRACE uncertainty is discussed in Section 5. TRACEv1 also assumed a preindustrial $x\text{CO}_2^{\text{atm}}$ of 280 ppm, which TRACE-Python makes more readily modifiable as an optional user input parameter, as described in Section 3.1.

90 This implementation of TRACE also retains its predecessor's estimated uncertainty of C_{anth} point estimates and inventories. Briefly, the estimated 1σ uncertainty of TRACE point estimates is the root sum of squared errors derived from a Monte Carlo analysis of error propagated from training data and error associated with a model reconstruction analysis (Carter et al., 2025). As with TRACEv1, the resulting uncertainty in C_{anth} likely underestimates the true reconstruction error in coastal, marginal, undersampled, and upwelling regions.

95 3 New Capabilities

In addition to its inherited capabilities, TRACE-Python adds several features which expand its scientific applications and provide more robust results. We divide these into two categories: practical improvements (Section 3.1) that improve user experience and applications, and fundamental improvements (Section 3.2) that may alter the results or interpretation of the method.

100 3.1 Practical Improvements

The practical function of TRACE is improved by an expanded array of optional user-accessible parameters to tune C_{anth} estimation. Now included in the main user-accessible function are options to adjust the shape of the IG-TTD distribution,



to specify preindustrial $x\text{CO}_2$, to change inorganic carbon equilibrium parameters (Humphreys et al., 2021, i.e. PyCO2SYS inputs), and to provide or reuse preformed properties. These parameters facilitate adaptation of TRACE to changing scientific 105 knowledge and needs, and create useful opportunities for comparison of the TRACE method with independent C_{anth} point estimates and inventories. Only the shape of the IG-TTD and the value of preindustrial $x\text{CO}_2$ will be explored in detail here, as their impacts on C_{anth} estimates are expected to be the greatest. Lastly, TRACE-Python is made more transparent and repeatable with self-describing output. A call to its main function returns a Climate and Forecast (CF) compliant (Hassell et al., 2017) dataset detailing all input and output parameters, their units, and details of the computing environment. These data may be 110 directly saved to the file system to facilitate data archiving and version control. This standardized and self-documenting format is expected to enhance the interpretation and portability of TRACE-Python.

The shape of the IG distribution is specified by the ratio of its second and first moments: Δ/Γ , such that larger values of this ratio increase the weight of older ages in the age distribution. The default value of the original and present implementations of TRACE is $\Delta/\Gamma = 1.3$ which has been found to minimize global mean error in ocean tracer simulations (He et al., 2018). 115 Previous work has found values of Δ/Γ between approximately 0.1-5 in different regions (Sonnerup et al., 2015), with a value around 1.0 having been frequently used in previous work estimating transport times and C_{anth} distributions with the IG-TTD method (Waugh et al., 2004, 2006). Other studies have found over-constrained satisfactory IG solutions to occupy a more restricted range of $0.2 \leq \Delta/\Gamma \leq 1.8$ (Stöven et al., 2015; Raimondi et al., 2024). Spatial variability of Δ/Γ and the evolving scientific knowledge of ocean circulation may be served by allowing TRACE users to vary Δ/Γ , to which end a demonstration 120 of its effect on estimated mean age and C_{anth} in a simulated transect and on the global C_{anth} inventory is given in Section 4.2. Internally, variability of Δ/Γ was enabled by retraining the neural networks estimating age distributions with IG shape characteristics constrained by discrete values $0.2 \leq \Delta/\Gamma \leq 1.8$ given in increments of 0.1, such that a user-provided Δ/Γ calls the age models of the nearest increment.

Preindustrial atmospheric $x\text{CO}_2$ is typically defined between approximately 275 and 290 ppm, depending on the reference 125 year defined as the beginning of the industrial era (Bronselaer et al., 2017). Differences in global C_{anth} inventories produced by TRACE under varying preindustrial $x\text{CO}_2$ conditions may be useful for reconciling literature estimates of C_{anth} inventories as well as global preindustrial ocean $x\text{CO}_2$ distributions. This iteration of TRACE makes preindustrial atmospheric $x\text{CO}_2$ accessible to the user in the main function, with a demonstration given in Section 4.2.

3.2 Fundamental Improvements

130 The results and interpretation of the TRACE method are improved by two changes: First, a new method for routine integration of point estimates into column inventories was introduced. Second, a more rigorous and rapid inorganic equilibrium calculation was incorporated into the C_{anth} estimation. The first change is external to the C_{anth} estimation, while the second is a core element of estimation. Together, these improvements allowed for the production of a revised global C_{anth} inventory and reevaluation of the TRACE method alongside other C_{anth} estimation methods.

135 A new integration routine was implemented to facilitate rapid and repeatable estimation of column C_{anth} inventories. Some methods for numerical interpolation and integration of sparse profile data may produce unrealistic column properties and



inventories from interpolation overshoots and discontinuities (Barker and McDougall, 2020), so the updated routine sought to avoid these qualities. A piecewise cubic hermite interpolation (Fritsch and Carlson, 1980) was performed between the most shallow and deepest C_{anth} estimate at each user-provided coordinate, followed by Romberg integration of the function 140 produced by interpolation (Romberg, 1955). This routine aims to resolve high gradients of C_{anth} profiles among water masses while remaining relatively insensitive to outliers and interpolation overshoots. The resulting column inventories may be easily summed across regions of interest to yield regional or global C_{anth} inventories. This function is provided in the TRACE-Python Github repository to promote repeatable column inventory estimation.

Inorganic carbon equilibrium calculation software was used for estimation of modern and preindustrial DIC as a function of 145 preformed properties and propagated CO_2 boundary conditions just as in TRACEv1, except for this updated TRACE method's use of PyCO2SYS (Humphreys et al., 2020), which did not require alteration of the solver function as was necessary for speed and performance in TRACEv1. Briefly, the iterative solution of the inorganic carbon system equilibria utilized by TRACEv1 via CO2SYS (version 1.1; van Heuven et al., 2011) was altered to increase the tolerance for pH change from 1×10^{-4} to 150 1×10^{-3} units, resulting in point estimates within the estimated uncertainties of TRACE. The extent to which TRACE-Python estimates differ from TRACEv1 due to the former's use of a more rigorous inorganic carbon equilibrium solver is discussed in Section 4. TRACE-Python utilized PyCO2SYS version 2.0.0 without alteration, and produced point estimates of C_{anth} for all 1.1×10^6 cells in the GLODAPv2.2016b gridded product for a single time step along the Historical/Linear CO_2 trajectory (see Section 4) in approximately 50 seconds (as the average of 10 runs) running on an Ubuntu 24.04.02 LTS machine with a 6-core Intel Core i5-9600K processor, versus approximately 60 seconds for the same estimation by TRACEv1 on the same hardware.

155 4 Assessment

Assessment of TRACE-Python sought to validate its comparability with TRACEv1, explore its sensitivity to new user parameter inputs, and finally to demonstrate its use alongside other ocean C_{anth} data products. All estimates were produced with TRACEv1 (Carter, 2025b) and TRACE-Python version 1.0.0, which was developed and hosted in a Github repository (Sandborn and Carter, 2025) containing its source code, instructions for installation, documentation, demonstration scripts, and status 160 badges indicating that the code passes internal consistency and validation tests. Comparability with TRACEv1 was established by calculation of check values as well as global gridded C_{anth} products using identical inputs. The two implementations were found to give identical results with precision approaching pmol kg^{-1} levels, which when integrated into regional and global inventories led to no significant difference. Sensitivity analysis of newly-accessible parameters demonstrated increased flexibility of the TRACE-Python routine and pointed towards new directions for method development and software application.

165 Check values given for TRACEv1 and TRACE-Python (Table 1) demonstrated results within their respective uncertainties. Precision between MATLAB and Python implementations was expected to vary depending on the exact data types and operations performed: both languages include double-precision floating point arithmetic by default, but other contributors to point estimate imprecision may be expected on the order of $10^{-5} \mu\text{mol kg}^{-1}$ from inorganic carbon equilibrium calculations alone (Humphreys et al., 2021).



Table 1. Check values for C_{anth} given by TRACE-Python and TRACEv1 (the original MATLAB implementation) for four combinations of year, salinity, and/or temperature. All values were generated for the coordinates 0°N 0°E at 0 m depth with salinity set to 35. The first two values assume SSP 5-3.4, while the second two values assume the Historical/Linear forcing. Missing temperature inputs as in the latter two check values were estimated from salinity and location using a neural network, which is not recommended for the most accurate behavior. The precision of both TRACE-Python and TRACEv1 estimates was limited to the magnitude of their differences, rather than that of their uncertainties.

Year	Temperature ($^{\circ}\text{C}$)	TRACE-Python ($\mu\text{mol kg}^{-1}$)	TRACEv1 C_{anth} ($\mu\text{mol kg}^{-1}$)	(TRACE-Python) – (TRACEv1) ($\mu\text{mol kg}^{-1}$)
2000	20	47.7868541	47.7868563	2.2×10^{-6}
2200	20	79.8749299	79.8749319	2.0×10^{-6}
2000	(<i>none provided</i>)	56.0591320	56.0591388	6.8×10^{-6}
2010	(<i>none provided</i>)	66.4566813	66.4566880	6.7×10^{-6}

170 A global gridded C_{anth} product was created using TRACE-Python, using seawater salinity, seawater temperature, coordinates, and depth from the GLODAPv2.2016b gridded product (Lauvset et al., 2016), which has a spatial resolution of $1^{\circ} \times 1^{\circ}$ and 33 depth horizons between the sea surface and 5500 m. Each of nine available atmospheric CO_2 pathways available in TRACE was employed to yield C_{anth} estimates for the years 1750, 1800, 1850, 1900, 1950, 1980, 1994.5, 2000, 2002.5, 2007.5, 2010, 2014.5, 2020, 2030, 2050, 2100, 2200, 2300, 2400, and 2500, chosen to align with previous literature global
175 C_{anth} inventory estimates. These global C_{anth} gridded estimates may be found in a Zenodo repository (Sandborn et al., 2025). Comparison of point C_{anth} estimates to the same analysis performed by TRACEv1 demonstrated agreement within uncertainties and approaching the limits of precision imposed by inorganic carbon equilibrium calculation. Their residuals (calculated as TRACEv1 estimates subtracted from TRACE-Python), across 9 atmospheric pathways, 20 timesteps, and 1.1×10^6 ocean cells in the GLODAPv2.2016b gridded product, demonstrated a median error of $-1.8 \times 10^{-6} \mu\text{mol kg}^{-1}$ and median absolute error
180 of $-2.6 \times 10^{-6} \mu\text{mol kg}^{-1}$. While the total range of error was -0.02 to $0.0005 \mu\text{mol kg}^{-1}$, 95% of absolute error was less than $6.4 \times 10^{-3} \mu\text{mol kg}^{-1}$. TRACE-Python underestimation (relative to TRACEv1) of the global distribution of C_{anth} was most apparent for cells with higher C_{anth} (Figure 2) which was repeatable for all CO_2 trajectories at all calculated times (Figures A1–A6). This apparent bias is consistent with the magnitude of expected precision of (MATLAB) CO2SYS versus PyCO2SYS as previously noted. Extrapolating the median error given above across the entire ocean yields a value on the order of 10^{-5} Pg ,
185 so we conclude that random or systematic biases existing between implementations of TRACE had no significant affect on inventories calculated using this gridded product, as demonstrated in the calculation of regional and global C_{anth} inventories below.

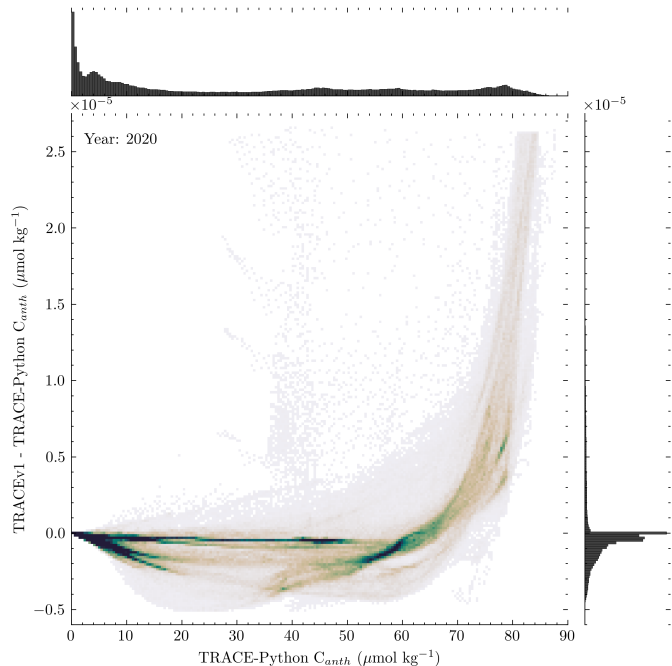


Figure 2. Histogram plot of 1.1×10^6 residuals of TRACEv1 and TRACE-Python point estimates of C_{anth} against TRACE-Python point estimates of C_{anth} performed on the GLODAPv2.2016b gridded product for the year 2020. Shading indicates relative density of residuals within a histogram cell, with darker colors indicating higher density. The ordinate (vertical) axis was limited to include 99% of point estimates. The median residual for 2020 was $-4.7 \times 10^{-7} \mu\text{mol kg}^{-1}$, the median absolute residual was $-8.7 \times 10^{-7} \mu\text{mol kg}^{-1}$, and the total range was $2.5 \times 10^{-4} - 5.7 \times 10^{-6} \mu\text{mol kg}^{-1}$. Note scaling of the ordinate by 10^{-5} , highlighting that the majority ($>83\%$) of residuals were within pmol kg $^{-1}$ range.

4.1 Global and regional inventories

Column inventories for the global C_{anth} gridded product were calculated using the integration method described in Section 190 3.2. Each $1^\circ \times 1^\circ$ cell of the sea surface grid was assigned a surface area as in Fay et al. (2021) and summed to give regional and global C_{anth} inventories using basin definitions after Fay and McKinley (2014) (Table 2). These inventories varied slightly from those given in (Carter et al., 2025) solely as a result of this work's improved integration method, and yielded a similar illustration of uneven storage of C_{anth} in the global ocean (Figure 3) in qualitative agreement with previous C_{anth} inventories. Applying the updated integration to the TRACEv1 gridded product yielded statistically-indistinguishable regional and global 195 C_{anth} inventories (Table C1) which were smaller than those of Carter et al. (2025) by approximately 7% for the period 1990-2015. Similarly, this integration was applied to the C_{anth} estimates in the GLODAPv2.2016b gridded product (Lauvset et al., 2024) for ease of comparison, yielding a global C_{anth} inventory of $164 \pm 29 \text{ Pg C}$ for the year 2002, which compares favorably with the inventory of $167 \pm 29 \text{ Pg C}$ given by Lauvset et al. (2020). In all cases, the improved inventory estimation approach yielded smaller inventory estimates that are, generally, more closely aligned with previous literature estimates. However, the



Table 2. Estimate of global and regional ocean C_{anth} inventories produced via TRACE-Python analysis of the GLODAPv2.2016b gridded product. Basins are defined after Fay and McKinley (2014). Values are given as Pg C $\pm 1\sigma$ uncertainty as for TRACEv1.

Year	Total C_{anth}	Pacific	Atlantic	Indian	Arctic	Southern
1750	-7.9 (-1.2)	-2.51 (-0.38)	-2.54 (-0.38)	-0.75 (-0.11)	-0.206 (-0.031)	-1.88 (-0.28)
1800	-6.43 (-0.97)	-2.03 (-0.30)	-1.97 (-0.30)	-0.551 (-0.083)	-0.125 (-0.019)	-1.76 (-0.26)
1850	-0.634 (-0.095)	0.086 (0.013)	-0.614 (-0.092)	0.0167 (0.0025)	0.0561 (0.0084)	-0.179 (-0.027)
1900	16.2 (2.4)	5.31 (0.80)	4.16 (0.62)	1.91 (0.29)	0.464 (0.070)	4.30 (0.65)
1950	52.2 (7.8)	16.7 (2.5)	14.1 (2.1)	5.85 (0.88)	1.33 (0.20)	14.2 (2.1)
1980	88 (13)	27.5 (4.1)	24.6 (3.7)	9.9 (1.5)	2.08 (0.31)	23.9 (3.6)
1994.5	117 (18)	36.1 (5.4)	33.5 (5.0)	13.4 (2.0)	2.74 (0.41)	31.6 (4.7)
2000	130 (19)	39.9 (6.0)	37.3 (5.6)	14.8 (2.2)	3.03 (0.45)	34.9 (5.2)
2002.5	136 (20)	41.8 (6.3)	39.1 (5.9)	15.5 (2.3)	3.17 (0.47)	36.5 (5.5)
2007.5	149 (22)	45.8 (6.9)	43.1 (6.5)	17.0 (2.6)	3.46 (0.52)	40.0 (6.0)
2010	156 (23)	47.9 (7.2)	45.0 (6.8)	17.8 (2.7)	3.62 (0.54)	41.8 (6.3)
2014.5	169 (25)	51.8 (7.8)	48.8 (7.3)	19.2 (2.9)	3.91 (0.59)	45.2 (6.8)
2020	186 (28)	57.0 (8.6)	53.8 (8.1)	21.2 (3.2)	4.30 (0.65)	49.8 (7.5)

200 decreases in the inventories were small relative to uncertainties and the updated TRACE global C_{anth} inventory with other previous data-based estimates (Figure 4) did not substantially or qualitatively alter the conclusions of Carter et al. (2025).

Agreement with DIC-based approaches (Sabine et al., 2004; Müller et al., 2023; Gruber et al., 2019) was good, while agreement with TTD- and inversion-based approaches (Davila et al., 2022; Lauvset et al., 2016; DeVries, 2014; Khatiwala et al., 2009; Waugh et al., 2006) remained more variable. In particular, the IG-TTD inventory estimate of Lauvset et al. (2016) 205 continued to be the most serious outlier, potentially due their differing treatment of atmospheric CO₂ disequilibrium, lack of SF₆ age constraint, and potentially other factors (cf. Section S9 Carter et al., 2025). The rate of C_{anth} accumulation over 1990-present was nearly identical in TRACE-Python global C_{anth} inventory compared to Davila et al. (2022), yet greater than given by DeVries (2014) despite the additional constraining role of the latter inversion in TRACE. Differences in the magnitude and rate of C_{anth} inventory change between the inversions of DeVries (2014) and Davila et al. (2022) are thought to be the result of 210 regional differences in circulation field strength constrained by different sets of tracers, and the same is likely true for TRACE; however, further investigation of representations of C_{anth} accumulation is beyond the scope of this work.

Projected global ocean C_{anth} inventories in Figure 4 (see also Table B1) indicated a range of potential outcomes of selected SSPs. The continued increase of each pathway's C_{anth} inventory through the year 2500 indicated continuing C_{anth} update by the ocean due to ventilation of presently-deep waters regardless of mitigation trajectory. Similarly, mapped column inventories 215 for future dates (Figure 3) demonstrated the increasingly unequal spatial distribution of ocean C_{anth} in the 21st century. In this way, TRACE provides a robust and accessible tool for exploring how mitigation efforts may be expressed in the past, present, and future ocean.

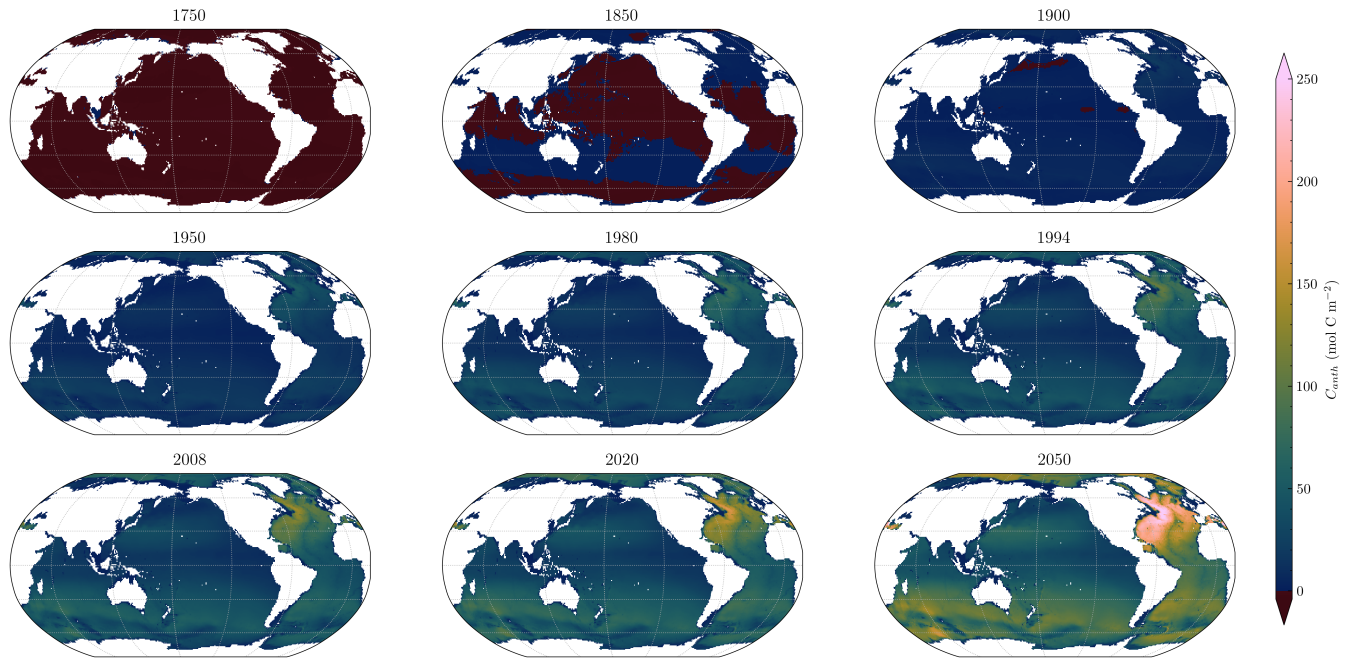


Figure 3. Column inventory of C_{anth} mapped for indicated years produced via TRACE analysis of the GLODAPv2.2016b gridded product assuming historical atmospheric CO_2 trajectory. Major C_{anth} sinks associated with deep water formation in the North Atlantic and Southern Oceans are visible in the propagation of elevated C_{anth} waters from these regions. Regions with negative column C_{anth} inventories were observed in the Pacific ocean until approximately 1900 due the imposition of a preindustrial xCO_2 definition of 280 ppm on old, deep waters formed under conditions of marginally lower xCO_2 .

4.2 User input sensitivity

Among the practical improvements accomplished in this work (Section 3.1) was the addition of a wider array of parameters 220 for C_{anth} estimation made accessible to the user. While this allowed for more flexibility in application, it necessitated improved understanding of the relationship between these parameters and TRACE C_{anth} estimates. To this end, we assessed the effects of altering two user-accessible parameters within reasonable bounds. This process illustrated sensitivity associated with parameter selection, explored the robustness of the method, and pointed to avenues of investigation which may improve the IG-TTD method and its comparability with other C_{anth} estimation methods.

225 The effect of shifting the preindustrial atmospheric CO_2 mixing fraction is to change the time at which ocean C_{anth} began accruing, and thus to alter C_{anth} inventories at all times before and after that point. To demonstrate this effect, C_{anth} global inventories were generated assuming historical atmospheric forcing as in Section 4.1, varying preindustrial atmospheric xCO_2 between 270 and 290 ppm (Figure 5a). The resulting set of inventories demonstrated a linear relationship with preindustrial atmospheric xCO_2 for any year, with a slope of approximately $-10 \text{ Pg C ppm}^{-1}$. This suggested a straightforward empirical 230 mechanism for comparing inventories performed on the basis of different preindustrial xCO_2 ; however, adjusting estimates

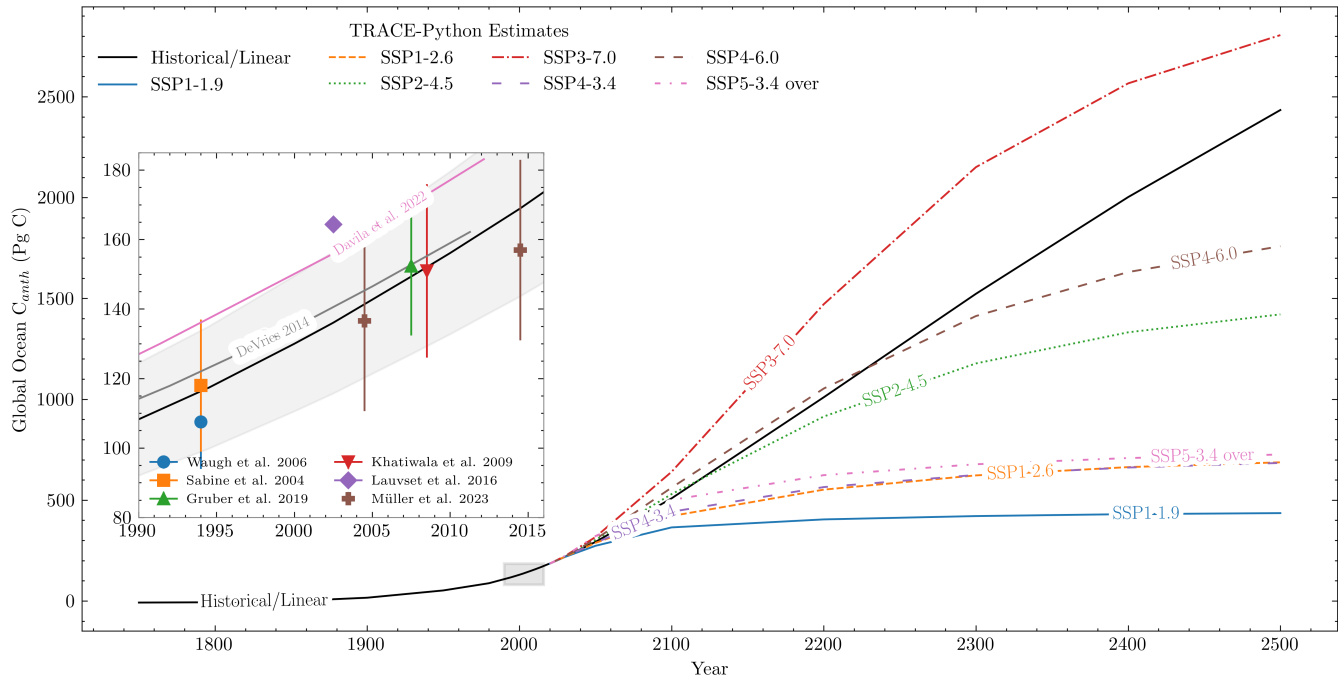


Figure 4. Global ocean C_{anth} inventories assuming indicated atmospheric CO_2 pathways produced via TRACE analysis of the GLO-DAPv2.2016b gridded product. Apparent kinks in the time series are due to TRACE estimation at widely-spaced points. Global ocean C_{anth} inventory estimates from the literature are shown with their uncertainties alongside the TRACE estimate in an inset figure, in which the uncertainty of the TRACE estimate is shown as a grey band. The estimate of Khatiwala et al. (2009) is shown with an 11 PgC increase to account for exclusion of the Arctic ocean as suggested in that work. The estimate of Waugh et al. (2006) is decreased by 20% to account for varying air-sea disequilibrium as suggested in that work. The estimate of Lauvset et al. (2016) published as the GLO-DAPv2.2016b gridded product was integrated using the same method as TRACE-Python, as described in Section 4.1.

performed on the basis of a preindustrial cutoff year introduces the additional step of converting the year to an atmospheric CO_2 fraction consistent with the atmospheric forcing of the method, which may not always be in evidence. As an example, the global ocean C_{anth} estimate of Khatiwala et al. (2009) was performed on the basis of a preindustrial cutoff year 1765, at which point the global annual mean atmospheric $x\text{CO}_2$ in this work was approximately 278 ppm. Adjusting this to a basis of 280 ppm would

235 involve a simple 20 Pg C decrease (or equivalently a 20 Pg C increase to TRACE), which would worsen agreement but maintain overlap in their respective uncertainties. This simple corrective mechanism is most suitable for qualitative demonstration, as it remains unclear how C_{anth} inventories in other works would shift were they carried out with higher or lower preindustrial atmospheric $x\text{CO}_2$ basis. Furthermore, some approaches do not integrate C_{anth} over regions of the ocean with low signal-to-uncertainty ratios, and the magnitude of this correction would decrease with the volume of the ocean considered. For these 240 reasons, previous C_{anth} inventory estimates in Figure 4 remain unadjusted. Shifting the baseline atmospheric $x\text{CO}_2$ (or year) of C_{anth} accumulation also changed the pre-industrial baseline of ocean $x\text{CO}_2$ which in volume-weighted distributions of TRACE

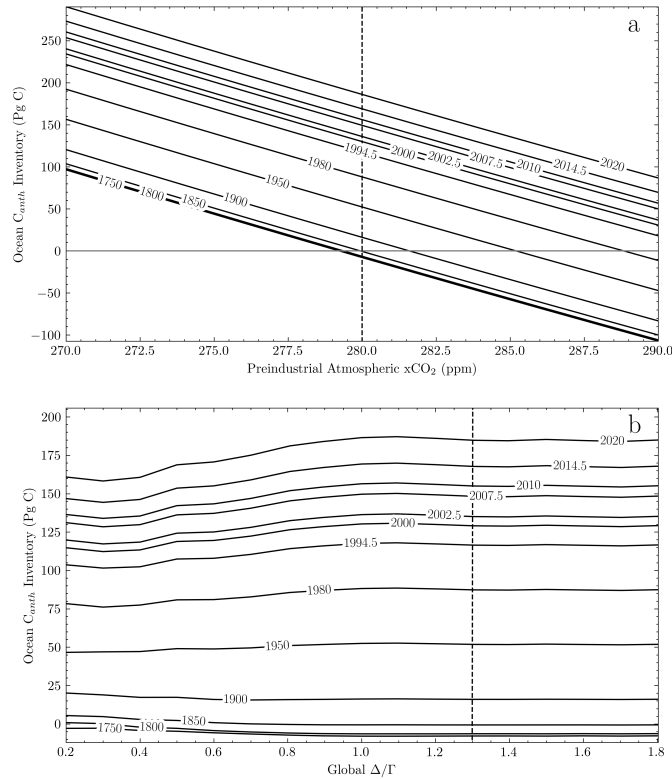


Figure 5. TRACE-estimated global ocean C_{anth} inventories at indicated years assuming: **a.** varying preindustrial atmospheric CO_2 concentrations or **b.** varying IG-TTD Δ/Γ . A linear relationship was expressed between preindustrial atmospheric CO_2 and all years' inventories. The relationship between Δ/Γ and ocean carbon C_{anth} inventories displayed asymptotic behavior, with sensitivity decreasing at high Δ/Γ . Vertical lines in both figures represent the TRACE defaults.

estimates broadened and increased from a narrow range of 276.95 ± 0.03 ppm (mean \pm s.d.) in 1750 C.E. to 280 ± 1 ppm in 1850 C.E. (Supplementary Section D). These values (and those of intermediate years) represent effective global ocean circulation-informed preindustrial xCO_2 distributions for common starting points of ocean state estimates. These sensitivity 245 analyses demonstrated the utility of TRACE to inform and compare C_{anth} inventories and pre-industrial inorganic carbon distributions in future work.

The shape of the IG-TTD age distribution may be modified by changing Δ/Γ , which by default is equal to 1.3. Increasing Δ/Γ increases the ratio of isopycnal diffusion to advection in the one-dimensional pipe flow framework of the IG solution (Waugh et al., 2003). The sensitivity of this parameter in TRACE was tested by varying Δ/Γ in increments of 0.1 between 0.2 250 and 1.8 in order to reconstruct C_{anth} global inventories assuming historical atmospheric forcing as in Section 4.1. The resulting global C_{anth} inventories increased with Δ/Γ up to 1.0, above which varying Δ/Γ had little effect on inventories (Figure 5b). This contrasts with the findings of He et al. (2018), which found decreasing C_{anth} inventories throughout $0.2 \leq \Delta/\Gamma \leq 1.8$. Regional variability of Δ/Γ poses a further problem which can be addressed with TRACE-Python.



In order to illustrate the regional effects of varying Δ/Γ , mean age and C_{anth} were estimated by TRACE along the WOCE 255 A16 transect using salinity, temperature, and coordinates from its 2013-2014 occupation by the CLIVAR program (CCHDO Hydrographic Data Office, 2023). Δ/Γ values of 0.4, 0.8, and 1.2 were chosen to span a domain of rapid C_{anth} change illustrated by Figure 5a, and the resulting hydrographic profiles (Figure 6) illustrated the expected inverse relationship of C_{anth} and mean age. Lower values of Δ/Γ were associated with higher vertical gradients as relatively “young” waters were confined to the 260 surface. Note that a single average value of Δ/Γ was imposed for all water masses in this example. The previously-noted spatial variability of Δ/Γ was not implemented, and is left to further research. Detailed hydrographic description and discussion of water masses and consequences of regional concentration of C_{anth} is beyond the scope of this work; instead, this sensitivity experiment demonstrates the potential for TRACE to test the effect of variable Δ/Γ on ocean mean age and C_{anth} . This demonstration also does not consider suitability of the IG-TTD framework to constrain age distribution for water masses with complex mixing regimes (cf. Stöven et al., 2015).

265 We conclude that varying Δ/Γ above approximately 1.0 will not lead to major changes in water mass age or C_{anth} as estimated by TRACE, but smaller values of Δ/Γ may lead to notable changes in mean age and C_{anth} distribution and inventory. Similarly, increasing preindustrial xCO_2 decreased C_{anth} inventories, suggesting a method for comparing the results of this routine with other products. The parameter tuning of the TRACE routine demonstrated here by varying preindustrial xCO_2 and Δ/Γ emphasized its flexibility, which may recommend it for further investigation of these parameters of the IG-TTD method.

270 **5 Discussion**

This work described an implementation of the TRACE method for the estimation of the ocean C_{anth} in Python, incorporating 275 several practical and fundamental improvements. The effect of these changes is to increase the accessibility and breadth of application of this tool, while providing a firmer scientific footing with clearer understanding of input parameter sensitivity. This updated version demonstrated equivalent function to the original product when given identical input, ensuring comparability across research products and users. The development of the TRACE method and its software implementations gains further currency when considered as part of a broader dialogue between scientific questions and research tools to address them. This work in particular has benefited from co-development with ESPER (and its predecessors) as a family of seawater property estimation methods of value to scientific, marine management, and earth observing communities, who may use these estimation routines to compare against observations, fill in unobserved regions, initialize models, and make informed management 280 decisions.

The practical and fundamental improvements to TRACE described and demonstrated in Section 3 provided an opportunity to test the sensitivity of TRACE to preindustrial xCO_2 and the shape of the TTD within the constraints of the IG framework. Global C_{anth} inventories were sensitive to both parameters within the range of values given by previous work. The spatial distribution of mean age and C_{anth} were similarly altered by Δ/Γ along a reconstructed meridional transect of the Atlantic 285 Ocean. Given the variability in inferred Δ/Γ associated with different water masses (cf. Sonnerup et al., 2015), future work using TRACE may investigate the interaction of regionally-varying Δ/Γ on water mass age and C_{anth} . This sensitivity analysis

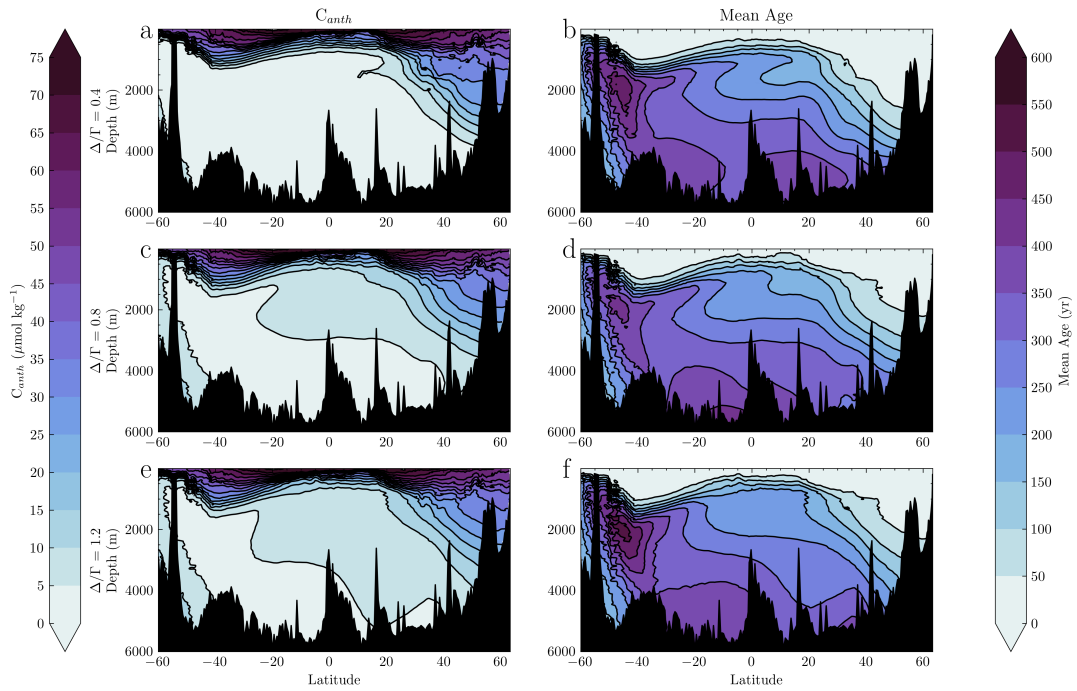


Figure 6. TRACE-estimated C_{anth} concentration (**a, c, e**) and mean age (**b, d, f**) along the WOCE A16 transect for the year 2013, calculated using three values of Δ/Γ spanning the range of greatest change in C_{anth} inventory. Higher values of Δ/Γ are associated with a higher surface-to-depth mean age gradient and less anthropogenic CO_2 invasion of the deep ocean at all latitudes.

of ocean C_{anth} and mean age to parameters of the TRACE method illustrates the importance of careful investigation of the assumptions of ocean state estimate routines. While TRACE-Python retains reasonable default values of these and other input parameters in common with TRACEv1, they are made accessible and tunable with the intention of aiding future investigation
 290 and expanding the applicability of this software tool.

Several other parameters and assumptions central to the TRACE method are not user-tunable, and consideration of these suggests room for continued method validation and improvement. In particular, its surface CO_2 disequilibrium does not vary in space, it prescribes transient tracer atmospheric saturation, C_{anth} is assumed to equal the entire change in DIC since the preindustrial era, it estimates preformed alkalinity and nutrients and assumes their invariance in time, and the IG-TTD implies
 295 steady state one dimensional pipe flow transport of transient signals into the ocean interior along isopycnals. A model-based review of uncertainties of the IG-TTD method found that transient tracer and C_{anth} saturations were the greatest contributors to uncertainty (He et al., 2018), so continued development of TRACE and other TTD-based ocean state estimation routines may be served by targeted investigation of the transient tracer and C_{anth} surface boundary conditions and their variability in time and space. Unfortunately, transient tracer saturations cannot yet be modified in TRACE without retraining its neural networks.

300 These shortcomings represent a continuing opportunity for comparing TRACE output with models and ocean observations.



We emphasize that TRACE, ESPER, and their seawater property estimation peers cannot replace observation; rather, they rely on continued monitoring providing the physical and chemical basis for accurate estimation. Ocean hydrography becomes increasingly-important in the face of climate change as Earth experiences extremes moving it outside its previously-observed state captured by property estimation routines. In light of the changing and improving picture of the ocean system to be 305 gained from future observations, TRACE will continue iteratively improving its estimation of C_{anth} . Future GLODAP releases will better constrain TTDs with the addition of more and better tracer constraints and preformed property estimates, while the advance of global ocean circulation and biogeochemical models may indicate more accurate parameterized relationships between the atmospheric anthropogenic CO_2 increase and its ocean sink.

6 Outlook

310 The development of TRACE has occurred in parallel to and in some cases dependent on related ocean chemistry software. This includes other property estimation routines (Carter et al., 2021a, b; Dias and Carter, 2025; Carter et al., 2017), inorganic carbon equilibrium and air-sea flux calculations (Humphreys et al., 2021; Sharp et al., 2020; Orr et al., 2015; Gregor and Humphreys, 2021; Lewis and Wallace, 1998) and seawater thermodynamic toolboxes (Firing et al., 2021). Further development of this suite of open-source software tools should seek to incorporate new findings and techniques, maintain dependency and 315 interoperability, and respond to the needs of users in order to pursue high-quality and accessible ocean chemistry data practices.

It is anticipated that TRACE will continue to be developed without fundamentally altering its core approach, while continuing to reliably offer results with well-documented assumptions and consistency across implementations. Potential directions for further development include integrating future GLODAP releases in its training data, including updated atmospheric CO_2 trajectories, and refining TTD shape and surface transient tracer and C_{anth} disequilibrium assumptions. As methods for estimating 320 C_{anth} continue use and development, a more comprehensive understanding of their differences, assumptions, and uncertainties should be formed. This need gains currency in light of the present need to understand the effects of climate change mitigation and marine carbon dioxide removal on the ocean carbon cycle. Future work in pursuit of these needs should seek to advance the practice of C_{anth} estimation from scientific and applied perspectives.

325 *Code and data availability.* The Python implementation of TRACE may be obtained at <https://doi.org/10.5281/zenodo.15597123> (Sandborn and Carter, 2025). The MATLAB implementation of TRACEv1 may be obtained at <https://doi.org/10.5281/zenodo.15692788> (Carter, 2025b). The GLODAPv2.2016b gridded product may be obtained at <https://www.nodc.noaa.gov/archive/arc0107/0162565/1.1/data/0-data/mapped> (Lauvset et al., 2016). The global C_{anth} gridded inventories produced in this work may be found at <https://doi.org/10.5281/zenodo.17246805> (Sandborn et al., 2025).



Appendix A: Gridded Product Comparison

330 The distribution of the differences, or residuals, of the TRACEv1 and TRACE-Python gridded data products indicated close agreement for results in 2020 (Figure 2). The same analysis produced for other years illustrates that this agreement holds for other periods as well (Figures A1-A6).

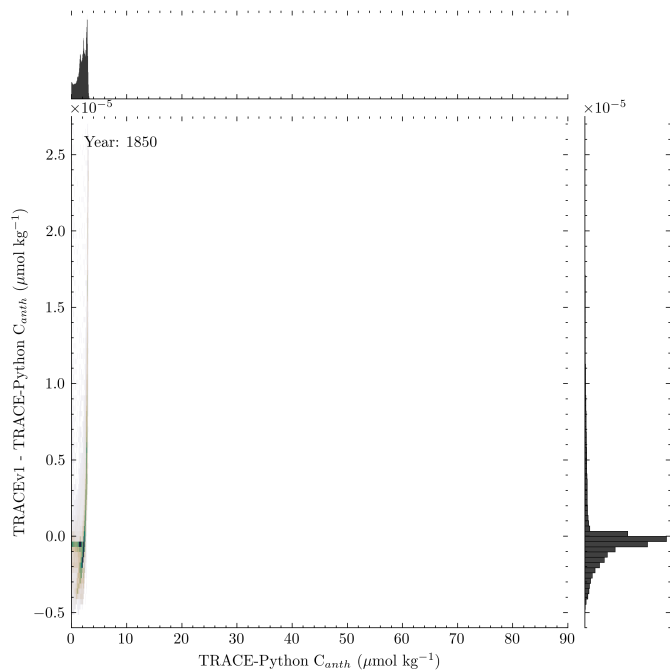


Figure A1. Histogram plot of the residuals of TRACEv1 and TRACE-Python point estimates of C_{anth} against TRACE-Python point estimates of C_{anth} performed on the GLODAPv2.2016b gridded product for the year 1850 given the historical CO₂ trajectory. The ordinate (vertical) axis was limited to include 0.99 of point estimates. Note scaling of the ordinate axis by 10⁻⁵.

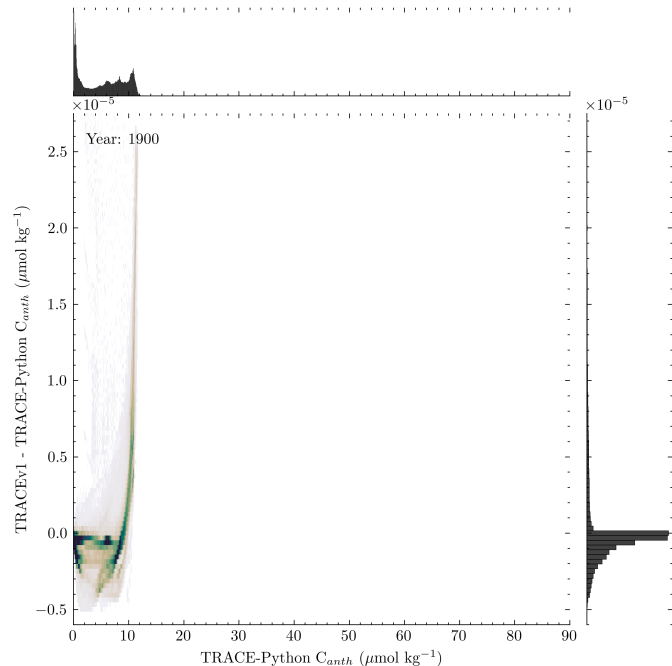


Figure A2. Histogram plot of the residuals of TRACEv1 and TRACE-Python point estimates of C_{anth} against TRACE-Python point estimates of C_{anth} performed on the GLODAPv2.2016b gridded product for the year 1900 given the historical CO₂ trajectory. The ordinate (vertical) axis was scaled as in Figure 2.

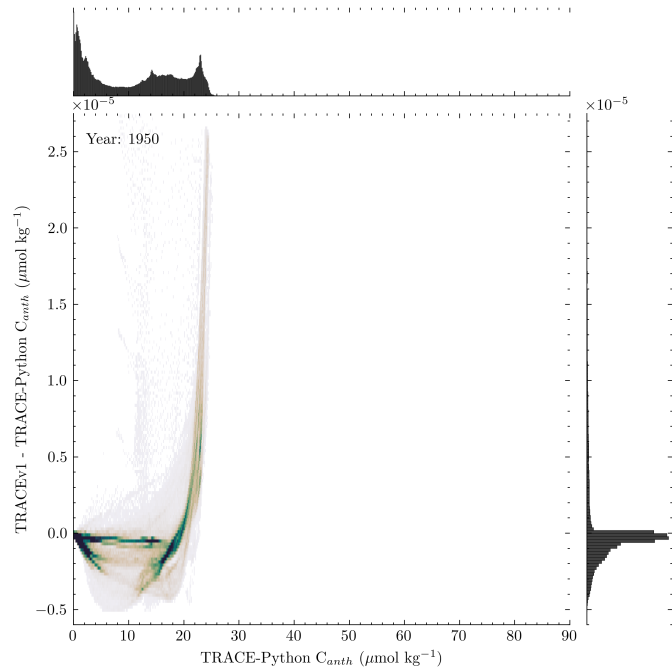


Figure A3. Histogram plot of the residuals of TRACEv1 and TRACE-Python point estimates of C_{anth} against TRACE-Python point estimates of C_{anth} performed on the GLODAPv2.2016b gridded product for the year 1950 given the historical CO₂ trajectory. The ordinate (vertical) axis was scaled as in Figure 2.

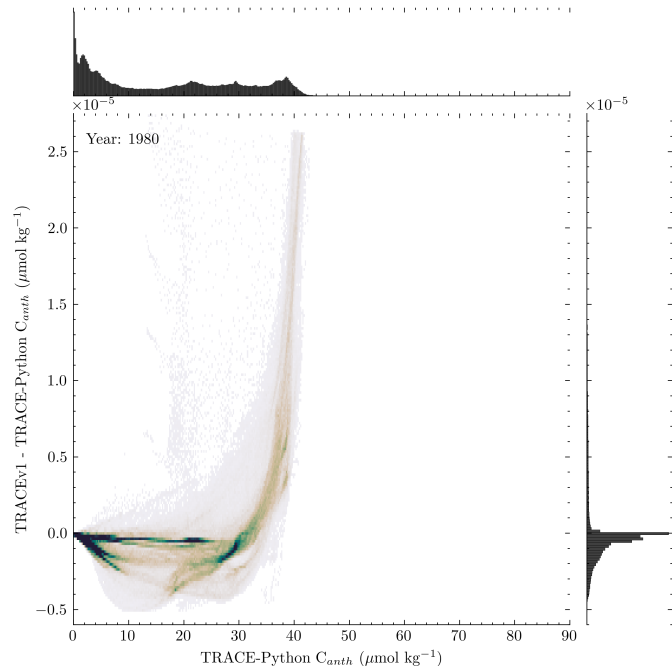


Figure A4. Histogram plot of the residuals of TRACEv1 and TRACE-Python point estimates of C_{anth} against TRACE-Python point estimates of C_{anth} performed on the GLODAPv2.2016b gridded product for the year 1980 given the historical CO₂ trajectory. The ordinate (vertical) axis was scaled as in Figure 2.

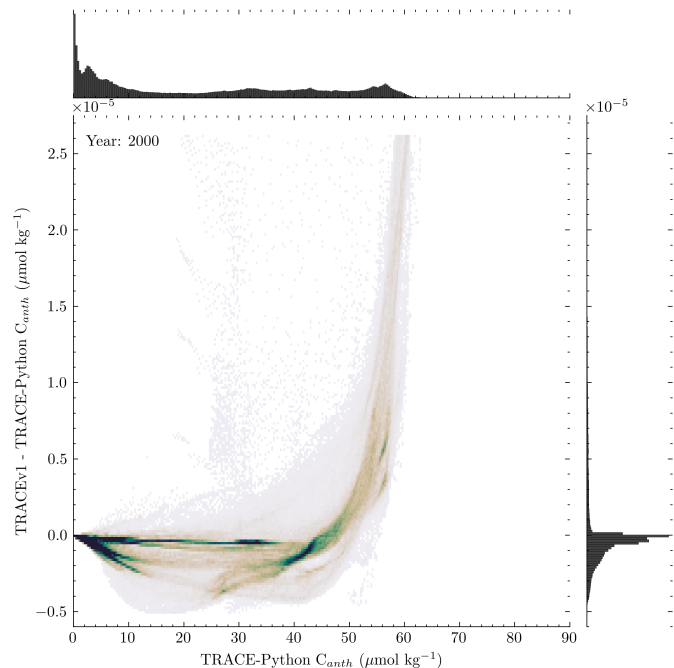


Figure A5. Histogram plot of the residuals of TRACEv1 and TRACE-Python point estimates of C_{anth} against TRACE-Python point estimates of C_{anth} performed on the GLODAPv2.2016b gridded product for the year 2000 given the historical CO₂ trajectory. The ordinate (vertical) axis was scaled as in Figure 2.

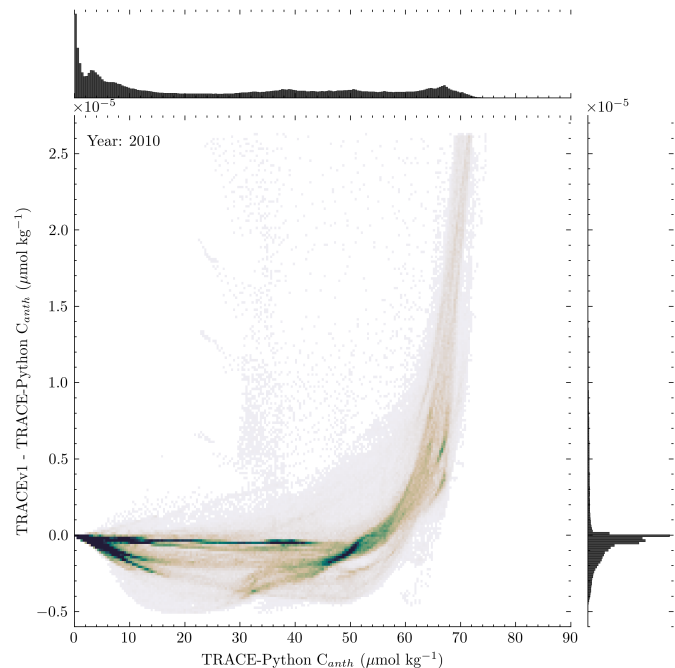


Figure A6. Histogram plot of the residuals of TRACEv1 and TRACE-Python point estimates of C_{anth} against TRACE-Python point estimates of C_{anth} performed on the GLODAPv2.2016b gridded product for the year 2010 given the historical CO₂ trajectory. The ordinate (vertical) axis was scaled as in Figure 2.



Appendix B: Projected C_{anth} Inventories

Among the strengths of TTD-based C_{anth} inventories is the ability to project forward and backward in time under certain
335 assumptions (Section 1). The inventories illustrated by Figure 4 after the year 2020 are given in Table B1 with uncertainties.

Table B1. Projections of global ocean C_{anth} inventories produced via TRACE analysis of the GLODAPv2.2016b gridded product under varying atmospheric CO₂ trajectories. Values are given as Pg C $\pm 1\sigma$ uncertainty.

	2030	2050	2100	2200	2300	2400	2500
Historical/Linear	219 (33)	293 (44)	509 (76)	1010 (150)	1520 (230)	2000 (300)	2430 (370)
SSP1-1.9	218 (33)	273 (41)	365 (55)	404 (61)	421 (63)	431 (65)	436 (65)
SSP1-2.6	220 (33)	288 (43)	421 (63)	552 (83)	623 (93)	664 (100)	690 (100)
SSP2-4.5	221 (33)	303 (45)	530 (79)	910 (140)	1180 (180)	1330 (200)	1420 (210)
SSP3-7.0	223 (33)	317 (48)	640 (96)	1470 (220)	2150 (320)	2570 (380)	2810 (420)
SSP3-7.0 lowNTCF	223 (33)	316 (47)	636 (95)	1460 (220)	2140 (320)	2560 (380)	2800 (420)
SSP4-3.4	219 (33)	289 (43)	442 (66)	565 (85)	625 (94)	662 (99)	680 (100)
SSP4-6.0	221 (33)	306 (46)	562 (84)	1050 (160)	1410 (210)	1630 (240)	1760 (260)
SSP5-3.4 over	223 (33)	322 (48)	501 (75)	624 (94)	680 (100)	710 (110)	730 (110)



Table C1. Estimate of global and regional ocean C_{anth} inventories produced via TRACEv1 analysis of the GLODAPv2.2016b gridded product and integration using the updated method. Basins are defined after Fay and McKinley (2014). Values are given as Pg C $\pm 1\sigma$ uncertainty.

Year	Total C_{anth}	Pacific	Atlantic	Indian	Arctic	Southern
1750	-7.9 (-1.2)	-2.51 (-0.38)	-2.54 (-0.38)	-0.75 (-0.11)	-0.206 (-0.031)	-1.88 (-0.28)
1800	-6.43 (-0.97)	-2.03 (-0.30)	-1.97 (-0.30)	-0.551 (-0.083)	-0.125 (-0.019)	-1.76 (-0.26)
1850	-0.634 (-0.095)	0.086 (0.013)	-0.614 (-0.092)	0.0167 (0.0025)	0.0561 (0.0084)	-0.179 (-0.027)
1900	16.2 (2.4)	5.31 (0.80)	4.16 (0.62)	1.91 (0.29)	0.464 (0.070)	4.30 (0.65)
1950	52.2 (7.8)	16.7 (2.5)	14.1 (2.1)	5.85 (0.88)	1.33 (0.20)	14.2 (2.1)
1980	88 (13)	27.5 (4.1)	24.6 (3.7)	9.9 (1.5)	2.08 (0.31)	23.9 (3.6)
1994.5	117 (18)	36.1 (5.4)	33.5 (5.0)	13.4 (2.0)	2.74 (0.41)	31.6 (4.7)
2000	130 (19)	39.9 (6.0)	37.3 (5.6)	14.8 (2.2)	3.03 (0.45)	34.9 (5.2)
2002.5	136 (20)	41.8 (6.3)	39.1 (5.9)	15.5 (2.3)	3.17 (0.47)	36.5 (5.5)
2007.5	149 (22)	45.8 (6.9)	43.1 (6.5)	17.0 (2.6)	3.46 (0.52)	40.0 (6.0)
2010	156 (23)	47.9 (7.2)	45.0 (6.8)	17.8 (2.7)	3.62 (0.54)	41.8 (6.3)
2014.5	169 (25)	51.8 (7.8)	48.8 (7.3)	19.2 (2.9)	3.91 (0.59)	45.2 (6.8)
2020	186 (28)	57.0 (8.6)	53.8 (8.1)	21.2 (3.2)	4.30 (0.65)	49.8 (7.5)
2030	219 (33)	67 (10)	63.2 (9.5)	24.8 (3.7)	5.06 (0.76)	58.8 (8.8)
2050	293 (44)	91 (14)	83 (13)	32.7 (4.9)	6.7 (1.0)	79 (12)
2100	509 (76)	159 (24)	141 (21)	55.3 (8.3)	11.0 (1.6)	143 (21)
2200	1010 (150)	300 (45)	289 (43)	111 (17)	18.7 (2.8)	291 (44)
2300	1520 (230)	419 (63)	477 (72)	175 (26)	24.8 (3.7)	427 (64)
2400	2000 (300)	515 (77)	680 (100)	237 (36)	29.7 (4.5)	542 (81)
2500	2430 (370)	594 (89)	870 (130)	294 (44)	33.9 (5.1)	640 (96)

Appendix C: Updated TRACEv1 C_{anth} Inventories

Application of the updated column and areal integration method described in this work (Section 3.2) to the original TRACEv1 gridded C_{anth} product (Carter, 2025a) yielded identical results to that produced in this work (Table 2), demonstrating their functional equivalence (Table C1).



340 **Appendix D: Preindustrial Ocean xCO₂ Distributions**

Volume weighted distributions of ocean xCO₂ were produced from the gridded data product described in this work (Sandborn et al., 2025) by performing a kernel density estimation analysis weighted by the volume of each cell in the product, along with summary statistics as reported in the main text (Section 3.2 and in the accompanying plot (Figure D1). Three years spanning the range of commonly-reported “pre-industrial” dates were considered, along with 2020 C.E. for comparison of the distributions.

345 The same distributions and statistics may be readily obtained from the published dataset for any year listed in the tables of this work, or for an intervening year by performing a TRACE analysis of the GLODAPv2.2016b or another suitable gridded product.

The extremely narrow distribution of ocean xCO₂ in Figure D1a resulted from the imposition of a CO₂ boundary condition given by Equation 2 on the pre-industrial stable atmospheric curve. Broadening and general increase of the distributions visible 350 in Figure D1b-d represents the propagation of that boundary condition through the global ocean, resulting in the present-day bimodal xCO₂ distribution representing highly-ventilated waters with xCO₂ approaching the atmospheric condition alongside poorly-ventilated waters maintaining xCO₂ little-removed from the pre-industrial state.

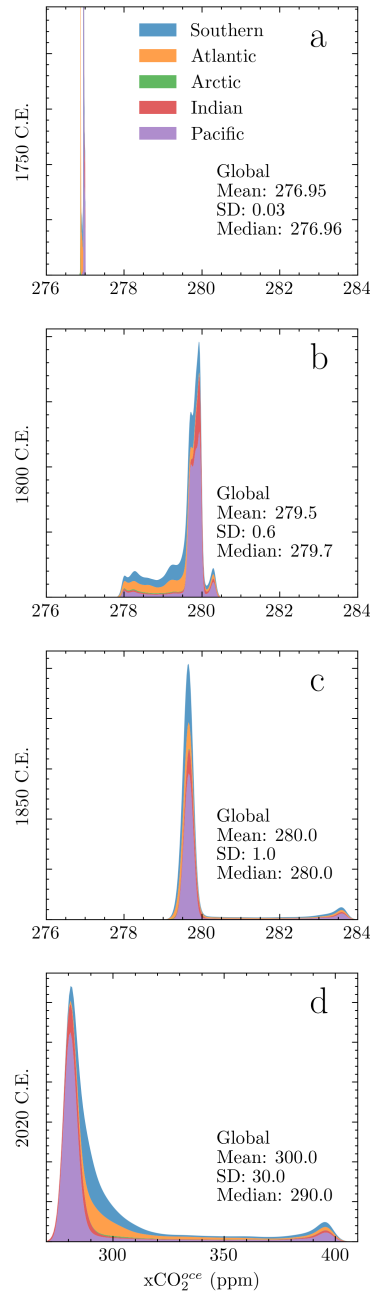


Figure D1. Volume-weighted kernel density estimates of ocean $x\text{CO}_2$ ($x\text{CO}_2^{\text{oce}}$) and summary statistics estimated for the global ocean by TRACE from the GLODAPv2.2016 gridded product temperature, salinity, and coordinates, colored and stacked by ocean basin defined as in the main text. **a, b, c:** $x\text{CO}_2$ distributions for the years 1750, 1800, 1850 C.E., illustrating the variability of ocean $x\text{CO}_2$ within the range of years previously given as “pre-industrial” starting points for ocean observational or modeling state estimation. **d:** $x\text{CO}_2$ distribution for the year 2020 C.E. provided for comparison. Note the horizontal coordinate is identical for **a, b, c** to aid comparison of distribution shifts, but extended for **d** to capture the broadened distribution.



355 *Author contributions.* DES was responsible for Python data product development, validation, formal analysis, investigation, data curation, writing, and visualization. BRC was responsible for original MATLAB data product development, project conceptualization, administration, code testing, and editing. ZKE and MJW were responsible for administration and editing. LMD tested portions of the code. Methods were devised by both DES and BRC.

Competing interests. The authors declare they have no conflict of interest.

360 *Acknowledgements.* DES is grateful to the NSF Division of Ocean Sciences (OCE) for support through the award entitled “Collaborative Research: US GOSHIP 2021-2026 Repeat Hydrography, Carbon, and Tracers” (OCE-2023545). MRC thanks the Global Ocean Monitoring and Observing program of NOAA for funding his time through the Carbon Data Management and Synthesis Program (Fund Ref. 100007298). Further thanks are due to Zach Erickson, Jörg Schwinger, Rolf Sonnerup, Andrea Fassbender, and Jonathan Sharp. The data used for transient tracer data products were collected and made freely available by GO-SHIP (<https://www.go-ship.org/>) and the national programs that contribute to it. This is Pacific Marine Environmental Laboratory (PMEL) contribution number 5824 and CICOES contribution number 2025-1506.



365 **References**

Archer, D., Kheshgi, H., and Maier-Reimer, E.: Dynamics of Fossil Fuel CO₂ Neutralization by Marine CaCO₃, *Global Biogeochem. Cycles*, 12, 259–276, <https://doi.org/10.1029/98GB00744>, 1998.

Barker, P. M. and McDougall, T. J.: Two Interpolation Methods Using Multiply-Rotated Piecewise Cubic Hermite Interpolating Polynomials, *Journal of Atmospheric and Oceanic Technology*, 37, 605–619, <https://doi.org/10.1175/JTECH-D-19-0211.1>, 2020.

370 Bronselaer, B., Winton, M., Russell, J., Sabine, C. L., and Khatiwala, S.: Agreement of CMIP5 Simulated and Observed Ocean Anthropogenic CO₂ Uptake, *Geophysical Research Letters*, 44, <https://doi.org/10.1002/2017gl074435>, 2017.

Bullister, J. L. and Warner, M. J.: Atmospheric Histories (1765–2022) for CFC-11, CFC-12, CFC-113, CCl₄, SF₆ and N₂O (NCEI Accession 0164584), https://doi.org/10.3334/CDIAC/OTG.CFC_ATM_HIST_2015, 2017.

Carter, B.: Anthropogenic Carbon Distributions from Preindustrial to 2500 c.e. Estimated Using Tracer-based Rapid Anthropogenic Carbon Estimation (Version 1), <https://doi.org/10.5281/ZENODO.15003059>, 2025a.

375 Carter, B. R.: BRCScienceProducts/TRACEv1: TRACEv1_publication, Zenodo, <https://doi.org/10.5281/ZENODO.15692788>, 2025b.

Carter, B. R., Feely, R. A., Williams, N. L., Dickson, A. G., Fong, M. B., and Takeshita, Y.: Updated Methods for Global Locally Interpolated Estimation of Alkalinity, pH, and Nitrate, *Limnology & Ocean Methods*, 16, 119–131, <https://doi.org/10.1002/lom3.10232>, 2017.

380 Carter, B. R., Bittig, H. C., Fassbender, A. J., Sharp, J. D., Takeshita, Y., Xu, Y.-Y., Álvarez, M., Wanninkhof, R., Feely, R. A., and Barbero, L.: New and Updated Global Empirical Seawater Property Estimation Routines, *Limnol Oceanogr Methods*, p. lom3.10461, <https://doi.org/10.1002/lom3.10461>, 2021a.

Carter, B. R., Feely, R. A., Lauvset, S. K., Olsen, A., DeVries, T., and Sonnerup, R.: Preformed Properties for Marine Organic Matter and Carbonate Mineral Cycling Quantification, *Global Biogeochem. Cycles*, 35, <https://doi.org/10.1029/2020GB006623>, 2021b.

385 Carter, B. R., Swinger, J., Sonnerup, R., Fassbender, A. J., Sharp, J. D., Dias, L. M., and Sandborn, D. E.: Tracer-Based Rapid Anthropogenic Carbon Estimation (TRACE), *Earth System Science Data*, 17, 3073–3088, <https://doi.org/10.5194/essd-17-3073-2025>, 2025.

CCHDO Hydrographic Data Office: CCHDO Hydrographic Data Archive, <https://doi.org/10.6075/J0CCHAM8>, 2023.

Clement, D. and Gruber, N.: The eMLR(C*) Method to Determine Decadal Changes in the Global Ocean Storage of Anthropogenic CO₂, *Global Biogeochemical Cycles*, 32, 654–679, <https://doi.org/10.1002/2017GB005819>, 2018.

390 Davila, X., Gebbie, G., Brakstad, A., Lauvset, S. K., McDonagh, E. L., Swinger, J., and Olsen, A.: How Is the Ocean Anthropogenic Carbon Reservoir Filled?, *Global Biogeochemical Cycles*, 36, e2021GB007055, <https://doi.org/10.1029/2021GB007055>, 2022.

DeVries, T.: The Oceanic Anthropogenic CO₂ Sink: Storage, Air-sea Fluxes, and Transports over the Industrial Era, *Global Biogeochemical Cycles*, 28, 631–647, <https://doi.org/10.1002/2013GB004739>, 2014.

395 DeVries, T., Yamamoto, K., Wanninkhof, R., Gruber, N., Hauck, J., Müller, J. D., Bopp, L., Carroll, D., Carter, B., Chau, T.-T.-T., Doney, S. C., Gehlen, M., Gloege, L., Gregor, L., Henson, S., Kim, J. H., Iida, Y., Ilyina, T., Landschützer, P., Le Quéré, C., Munro, D., Nissen, C., Patara, L., Pérez, F. F., Resplandy, L., Rodgers, K. B., Swinger, J., Séférian, R., Sicardi, V., Terhaar, J., Triñanes, J., Tsujino, H., Watson, A., Yasunaka, S., and Zeng, J.: Magnitude, Trends, and Variability of the Global Ocean Carbon Sink From 1985 to 2018, *Global Biogeochemical Cycles*, 37, e2023GB007780, <https://doi.org/10.1029/2023GB007780>, 2023.

Dias, L. M. and Carter, B. R.: PyESPERv1.01.01: A Python Implementation of Empirical Seawater Property Estimation Routines (ESPERs), <https://doi.org/10.5194/egusphere-2025-458>, 2025.

400 Doney, S. C., Busch, D. S., Cooley, S. R., and Kroeker, K. J.: The Impacts of Ocean Acidification on Marine Ecosystems and Reliant Human Communities, *Annu. Rev. Environ. Resour.*, 45, 83–112, <https://doi.org/10.1146/annurev-environ-012320-083019>, 2020.



Fay, A. R. and McKinley, G. A.: Global Open-Ocean Biomes: Mean and Temporal Variability, *Earth Syst. Sci. Data*, 6, 273–284, <https://doi.org/10.5194/essd-6-273-2014>, 2014.

Fay, A. R., Gregor, L., Landschützer, P., McKinley, G. A., Gruber, N., Gehlen, M., Iida, Y., Laruelle, G. G., Rödenbeck, C., Roobaert, A., and Zeng, J.: SeaFlux: Harmonization of Air–Sea CO₂ Fluxes from Surface pCO₂data Products Using a Standardized Approach, *Earth Syst. Sci. Data*, 13, 4693–4710, <https://doi.org/10.5194/essd-13-4693-2021>, 2021.

Firing, E., Filipe, Barna, A., and Abernathey, R.: TEOS-10/GSW-Python: V3.4.1, Zenodo, <https://doi.org/10.5281/zenodo.4631364>, 2021.

Friedlingstein, P., O’Sullivan, M., Jones, M. W., Andrew, R. M., Bakker, D. C. E., Hauck, J., Landschützer, P., Le Quéré, C., Luijckx, I. T., Peters, G. P., Peters, W., Pongratz, J., Schwingshakl, C., Sitch, S., Canadell, J. G., Ciais, P., Jackson, R. B., Alin, S. R., Anthoni, P., Barbero, L., Bates, N. R., Becker, M., Bellouin, N., Decharme, B., Bopp, L., Brasika, I. B. M., Cadule, P., Chamberlain, M. A., Chandra, N., Chau, T.-T.-T., Chevallier, F., Chini, L. P., Cronin, M., Dou, X., Enyo, K., Evans, W., Falk, S., Feely, R. A., Feng, L., Ford, D. J., Gasser, T., Ghattas, J., Gkrizalis, T., Grassi, G., Gregor, L., Gruber, N., Gürses, Ö., Harris, I., Hefner, M., Heinke, J., Houghton, R. A., Hurtt, G. C., Iida, Y., Ilyina, T., Jacobson, A. R., Jain, A., Jarníková, T., Jersild, A., Jiang, F., Jin, Z., Joos, F., Kato, E., Keeling, R. F., Kennedy, D., Klein Goldewijk, K., Knauer, J., Korsbækken, J. I., Kötzinger, A., Lan, X., Lefèvre, N., Li, H., Liu, J., Liu, Z., Ma, L., Marland, G., Mayot, N., McGuire, P. C., McKinley, G. A., Meyer, G., Morgan, E. J., Munro, D. R., Nakaoka, S.-I., Niwa, Y., O’Brien, K. M., Olsen, A., Omar, A. M., Ono, T., Paulsen, M., Pierrot, D., Pocock, K., Poulter, B., Powis, C. M., Rehder, G., Resplandy, L., Robertson, E., Rödenbeck, C., Rosan, T. M., Schwinger, J., Séférian, R., Smallman, T. L., Smith, S. M., Sospedra-Alfonso, R., Sun, Q., Sutton, A. J., Sweeney, C., Takao, S., Tans, P. P., Tian, H., Tilbrook, B., Tsujino, H., Tubiello, F., Van Der Werf, G. R., Van Ooijen, E., Wanninkhof, R., Watanabe, M., Wimart-Rousseau, C., Yang, D., Yang, X., Yuan, W., Yue, X., Zaehle, S., Zeng, J., and Zheng, B.: Global Carbon Budget 2023, *Earth Syst. Sci. Data*, 15, 5301–5369, <https://doi.org/10.5194/essd-15-5301-2023>, 2023.

Fritsch, F. N. and Carlson, R. E.: Monotone Piecewise Cubic Interpolation, *SIAM J. Numer. Anal.*, 17, 238–246, <https://doi.org/10.1137/0717021>, 1980.

Gregor, L. and Humphreys, M. P.: SeaFlux: Updated Continuous Integration and Docs, Zenodo, <https://doi.org/10.5281/ZENODO.4659162>, 2021.

Gruber, N., Sarmiento, J. L., and Stocker, T. F.: An Improved Method for Detecting Anthropogenic CO₂ in the Oceans, *Global Biogeochemical Cycles*, 10, 809–837, <https://doi.org/10.1029/96GB01608>, 1996.

Gruber, N., Clement, D., Carter, B. R., Feely, R. A., Van Heuven, S., Hoppema, M., Ishii, M., Key, R. M., Kozyr, A., Lauvset, S. K., Lo Monaco, C., Mathis, J. T., Murata, A., Olsen, A., Perez, F. F., Sabine, C. L., Tanhua, T., and Wanninkhof, R.: The Oceanic Sink for Anthropogenic CO₂ from 1994 to 2007, *Science*, 363, 1193–1199, <https://doi.org/10.1126/science.aau5153>, 2019.

Haine, T. W. N., Griffies, S. M., Gebbie, G., and Jiang, W.: A Review of Green’s Function Methods for Tracer Timescales and Pathways in Ocean Models, *J Adv Model Earth Syst.*, 17, e2024MS004637, <https://doi.org/10.1029/2024MS004637>, 2025.

Hall, T. M., Haine, T. W. N., and Waugh, D. W.: Inferring the Concentration of Anthropogenic Carbon in the Ocean from Tracers, *Global Biogeochemical Cycles*, 16, <https://doi.org/10.1029/2001GB001835>, 2002.

Hassell, D., Gregory, J., Blower, J., Lawrence, B. N., and Taylor, K. E.: A Data Model of the Climate and Forecast Metadata Conventions (CF-1.6) with a Software Implementation (Cf-Python v2.1), *Geosci. Model Dev.*, 10, 4619–4646, <https://doi.org/10.5194/gmd-10-4619-2017>, 2017.

He, Y.-C., Tjiputra, J., Langehaug, H. R., Jeansson, E., Gao, Y., Schwinger, J., and Olsen, A.: A Model-Based Evaluation of the Inverse Gaussian Transit-Time Distribution Method for Inferring Anthropogenic Carbon Storage in the Ocean, *JGR Oceans*, 123, 1777–1800, <https://doi.org/10.1002/2017JC013504>, 2018.



440 Holzer, M. and Primeau, F. W.: Improved Constraints on Transit Time Distributions from Argon 39: A Maximum Entropy Approach, *J. Geophys. Res.*, 115, 2010JC006410, <https://doi.org/10.1029/2010JC006410>, 2010.

Humphreys, M. P., Sandborn, D. E., Gregor, L., Pierrot, D., van Heuven, S., S.M.A.C., Lewis, E., and Wallace, D.: PyCO2SYS: Marine Carbonate System Calculations in Python, Zenodo, <https://doi.org/10.5281/zenodo.3744275>, 2020.

Humphreys, M. P., Lewis, E. R., Sharp, J. D., and Pierrot, D.: PyCO2SYS v1.7: Marine Carbonate System Calculations in Python, Preprint, 445 *Oceanography*, <https://doi.org/10.5194/gmd-2021-159>, 2021.

Jiang, L.-Q., Dunne, J., Carter, B. R., Tjiputra, J. F., Terhaar, J., Sharp, J. D., Olsen, A., Alin, S., Bakker, D. C. E., Feely, R. A., Gattuso, J.-P., Hogan, P., Ilyina, T., Lange, N., Lauvset, S. K., Lewis, E. R., Lovato, T., Palmieri, J., Santana-Falcón, Y., Schwinger, J., Séférian, R., Strand, G., Swart, N., Tanhua, T., Tsujino, H., Wanninkhof, R., Watanabe, M., Yamamoto, A., and Ziehn, T.: Global Surface Ocean Acidification Indicators From 1750 to 2100, *J Adv Model Earth Syst.*, 15, e2022MS003563, <https://doi.org/10.1029/2022MS003563>, 450 2023.

Keeling, R. F. and Keeling, C. D.: Atmospheric Monthly in Situ CO₂ Data - Mauna Loa Observatory, Hawaii, <https://doi.org/10.6075/J08W3BHW>, 2017.

Khatiwala, S., Primeau, F., and Hall, T.: Reconstruction of the History of Anthropogenic CO₂ Concentrations in the Ocean, *Nature*, 462, 346–349, <https://doi.org/10.1038/nature08526>, 2009.

455 Khatiwala, S., Tanhua, T., Mikaloff Fletcher, S., Gerber, M., Doney, S. C., Graven, H. D., Gruber, N., McKinley, G. A., Murata, A., Ríos, A. F., and Sabine, C. L.: Global Ocean Storage of Anthropogenic Carbon, *Biogeosciences*, 10, 2169–2191, <https://doi.org/10.5194/bg-10-2169-2013>, 2013.

Lauvset, S. K., Key, R. M., Olsen, A., van Heuven, S., Velo, A., Lin, X., Schirnick, C., Kozyr, A., Tanhua, T., Hoppema, M., Jutterström, S., 460 Steinfeldt, R., Jeansson, E., Ishii, M., Perez, F. F., Suzuki, T., and Watelet, S.: A New Global Interior Ocean Mapped Climatology: The 10 × 10 GLODAP Version 2, *Earth Syst. Sci. Data*, 2016.

Lauvset, S. K., Carter, B. R., Pérez, F. F., Jiang, L.-Q., Feely, R. A., Velo, A., and Olsen, A.: Processes Driving Global Interior Ocean pH Distribution, *Global Biogeochemical Cycles*, 34, e2019GB006229, <https://doi.org/10.1029/2019GB006229>, 2020.

Lauvset, S. K., Lange, N., Tanhua, T., Bittig, H. C., Olsen, A., Kozyr, A., Álvarez, M., Azetsu-Scott, K., Brown, P. J., Carter, B. R., Cotrim Da Cunha, L., Hoppema, M., Humphreys, M. P., Ishii, M., Jeansson, E., Murata, A., Müller, J. D., Pérez, F. F., Schirnick, C., Steinfeldt, 465 R., Suzuki, T., Ulfsbo, A., Velo, A., Woosley, R. J., and Key, R. M.: The Annual Update GLODAPv2.2023: The Global Interior Ocean Biogeochemical Data Product, *Earth Syst. Sci. Data*, 16, 2047–2072, <https://doi.org/10.5194/essd-16-2047-2024>, 2024.

Lewis, E. and Wallace, D.: Program Developed for CO₂ System Calculations, *Tech. Rep. ORNL/CDIAC-105*, Oak Ridge Natl. Lab., Oak Ridge, Tenn., 1998.

Meinshausen, M., Nicholls, Z. R. J., Lewis, J., Gidden, M. J., Vogel, E., Freund, M., Beyerle, U., Gessner, C., Nauels, A., Bauer, N., Canadell, 470 J. G., Daniel, J. S., John, A., Krummel, P. B., Luderer, G., Meinshausen, N., Montzka, S. A., Rayner, P. J., Reimann, S., Smith, S. J., van den Berg, M., Velders, G. J. M., Vollmer, M. K., and Wang, R. H. J.: The Shared Socio-Economic Pathway (SSP) Greenhouse Gas Concentrations and Their Extensions to 2500, *Geosci. Model Dev.*, 13, 3571–3605, <https://doi.org/10.5194/gmd-13-3571-2020>, 2020.

Müller, J. D., Gruber, N., Carter, B., Feely, R., Ishii, M., Lange, N., Lauvset, S. K., Murata, A., Olsen, A., Pérez, F. F., Sabine, C., Tanhua, T., Wanninkhof, R., and Zhu, D.: Decadal Trends in the Oceanic Storage of Anthropogenic Carbon From 1994 to 2014, *AGU Advances*, 475 4, e2023AV000875, <https://doi.org/10.1029/2023AV000875>, 2023.

Orr, J. C., Epitalon, J.-M., and Gattuso, J.-P.: Comparison of Ten Packages That Compute Ocean Carbonate Chemistry, *Biogeosciences*, 12, 1483–1510, <https://doi.org/10.5194/bg-12-1483-2015>, 2015.



Raimondi, L., Wefing, A.-M., and Casacuberta, N.: Anthropogenic Carbon in the Arctic Ocean: Perspectives From Different Transient Tracers, *JGR Oceans*, 129, e2023JC019999, <https://doi.org/10.1029/2023JC019999>, 2024.

480 Romberg, W.: Vereinfachte Numerische Integration, *Det Kongelige Norske Videnskabers Selskab Forhandlinger*, 28, 1955.

Rubino, M., Etheridge, D., Thornton, D., Allison, C., Francey, R., Langenfelds, R., Steele, P., Trudinger, C., Spencer, D., Curran, M., Van Ommen, T., and Smith, A.: Law Dome Ice Core 2000-Year CO₂, CH₄, N₂O and d¹³C-CO₂, <https://doi.org/10.25919/5BFE29FF807FB>, 2019.

Sabine, C. L., Feely, R. A., Gruber, N., Key, R. M., Lee, K., Bullister, J. L., Wanninkhof, R., Wong, C. S., Wallace, D. W. R., Tilbrook, B., Millero, F. J., Peng, T.-H., Kozyr, A., Ono, T., and Rios, A. F.: The Oceanic Sink for Anthropogenic CO₂, *Science*, 305, 367–371, <https://doi.org/10.1126/science.1097403>, 2004.

485 Sandborn, D. and Carter, B.: Tracer-Based Rapid Anthropogenic Carbon Estimation (TRACEv0.1.0-Python), Zenodo, <https://doi.org/10.5281/ZENODO.15597123>, 2025.

Sandborn, D., Carter, B., Warner, M. J., Erickson, Z., and Dias, L.: Global Ocean Anthropogenic Carbon Concentrations from Preindustrial to 2500 c.e. Estimated Using TRACE-Python, <https://doi.org/10.5281/zenodo.17246805>, 2025.

490 Sharp, J. D., Pierrot, D., Humphreys, M. P., Epitalon, J.-M., Orr, J. C., Lewis, E. R., and Wallace, D. W.: CO₂SYsV3 for MATLAB, Zenodo, <https://doi.org/10.5281/ZENODO.3952803>, 2020.

Sonnerup, R. E., Mecking, S., Bullister, J. L., and Warner, M. J.: Transit Time Distributions and Oxygen Utilization Rates from Chlorofluorocarbons and Sulfur Hexafluoride in the Southeast Pacific Ocean, *JGR Oceans*, 120, 3761–3776, <https://doi.org/10.1002/2015JC010781>, 2015.

495 Stöven, T., Tanhua, T., Hoppema, M., and Bullister, J. L.: Perspectives of Transient Tracer Applications and Limiting Cases, *Ocean Sci.*, 11, 699–718, <https://doi.org/10.5194/os-11-699-2015>, 2015.

van Heuven, S., Pierrot, D., Rae, J., Lewis, E., and Wallace, D.: CO₂SYsV1.1, MATLAB Program Developed for CO₂ System Calculations, ORNL/CDIAC-105b. Carbon Dioxide Information Analysis Center, Oak Ridge National Laboratory, U.S. DoE, Oak Ridge, TN., 2011.

Waugh, D. W., Hall, T. M., and Haine, T. W. N.: Relationships among Tracer Ages, *J. Geophys. Res.*, 108, 2002JC001325, <https://doi.org/10.1029/2002JC001325>, 2003.

500 Waugh, D. W., Haine, T. W., and Hall, T. M.: Transport Times and Anthropogenic Carbon in the Subpolar North Atlantic Ocean, *Deep Sea Research Part I: Oceanographic Research Papers*, 51, 1475–1491, <https://doi.org/10.1016/j.dsr.2004.06.011>, 2004.

Waugh, D. W., Hall, T. M., McNeil, B. I., Key, R., and Matear, R. J.: Anthropogenic CO₂ in the Oceans Estimated Using Transit Time Distributions, *Tellus B: Chemical and Physical Meteorology*, 58, 376, <https://doi.org/10.1111/j.1600-0889.2006.00222.x>, 2006.